PSFC/JA-04-9

Using nuclear data and Monte-Carlo techniques to study areal density and mix in D_2 implosions

S. Kurebayash, J. A. Frenje, F. H. Séguin, J. R. Rygg,
C. K. Li, R. D. Petrasso, V. Yu. Glebov[1],
J. A. Delettrez[1], T. C. Sangster[1], D. D. Meyerhofer[1],
C. Stoeckl[1], J. M. Soures[1], P. A. Amendt[2],
S. P. Hatchett[2], and R. E. Turner[2]

5 March 2004

Plasma Science and Fusion Center
Massachusetts Institute of Technology
Cambridge, MA 02139 USA

Laboratory for Laser Energetics, University of Rochester
Rochester, NY 14623 USA

Lawrence Livermore National Laboratory
Livermore, CA 94550 USA

This work described here was performed in part at the LLE National Laser Users' Facility (NLUF), and was supported in part by the US DoE (grant DE-FG03-03SF22691), US DoE DP/NNSA (Cooperative Agreement DE-FG03-03NA00058), LLE (subcontract 412160-001G), and LLNL (subcontract B504974).

Submitted for publication to *Physics of Plasmas.*

Using nuclear data and Monte-Carlo techniques to study areal density and mix in D_2 implosions

S. Kurebayashi, J. A. Frenje, F. H. Séguin, J. R. Rygg, C. K. Li, and R. D. Petrasso[a)]

Plasma Science and Fusion Center, Massachusetts Institute of Technology, Cambridge, Massachusetts 02139

V. Yu. Glebov, J. A. Delettrez, T. C. Sangster, D. D. Meyerhofer[b)], C. Stoeckl, and J. M. Soures

Laboratory for Laser Energetics, University of Rochester, Rochester, New York 14623

P. A. Amendt, S. P. Hatchett, and R. E. Turner

Lawrence Livermore National Laboratory, Livermore, California 94550

ABSTRACT

Measurements from three classes of direct-drive implosions at the OMEGA laser system [T. R. Boehly *et al.*, Opt. Commun. **133**, 495 (1997)] were combined with Monte-Carlo simulations to investigate models for determining hot-fuel areal density (ρR_{hot}) in compressed, D_2-filled capsules, and to assess the impact of mix and other factors on the determination of ρR_{hot}. The results of the Monte-Carlo calculations were compared to predictions of simple commonly used models that use ratios of either secondary D^3He proton yields or secondary DT neutron yields to primary DD neutron yields to provide estimates $\rho R_{hot,p}$ or $\rho R_{hot,n}$, respectively, for ρR_{hot}. For the first class of implosions, where ρR_{hot} is low ($\leq$ 3 mg/cm^2), $\rho R_{hot,p}$ and $\rho R_{hot,n}$ often agree with each other and are often good estimates of the actual ρR_{hot}. For the second class of implosions, where ρR_{hot} is of order 10 mg/cm^2, $\rho R_{hot,p}$ often underestimates the actual value due to secondary proton yield saturation. In addition, fuel-shell mix causes $\rho R_{hot,p}$ to further underestimate, and $\rho R_{hot,n}$ to overestimate, ρR_{hot}. As a result, values of $\rho R_{hot,p}$ and $\rho R_{hot,n}$ can be interpreted as lower and upper limits, respectively. For the third class of implosions, involving cryogenic capsules, secondary protons and neutrons are produced mainly in the hot and cold fuel regions, respectively, and the effects of the mixing of hot and cold fuel must be taken into account when interpreting the values of $\rho R_{hot,p}$ and $\rho R_{hot,n}$. From these data sets, we conclude that accurate inference of ρR_{hot} requires comprehensive measurements in combination with detailed modeling.

a) Also visiting Senior Scientist, Laboratory for Laser Energetics, University of Rochester.

b) Also Department of Mechanical Engineering, Physics and Astronomy.

I. INTRODUCTION

Maximizing the hot-fuel areal density (ρR_{hot}) and understanding the effects of mix upon it are fundamental issues of inertial confinement fusion (ICF).[1-3] One method used to estimate ρR_{hot} of D_2-filled capsule implosions is to measure the yields of secondary protons (Y_{2p}) and/or secondary neutrons (Y_{2n}) relative to the primary neutron yield (Y_{1n}).[4-12] These secondary particles result from sequential reactions in which the energetic primary products of reactions,

$$D + D \rightarrow n(2.45\ MeV) + {}^3He(0.82\ MeV), \quad (1)$$

$$D + D \rightarrow p(3.02\ MeV) + T(1.01\ MeV), \quad (2)$$

undergo fusion reactions with thermal deuterons in the fuel

$${}^3He(\leq 0.82\ MeV) + D \rightarrow p(12.5 - 17.4\ MeV) + {}^4He(6.6 - 1.7\ MeV), \quad (3)$$

$$T(\leq 1.01\ MeV) + D \rightarrow n(11.9 - 17.2\ MeV) + {}^4He(6.7 - 1.4\ MeV). \quad (4)$$

These processes produce secondary particles with spectra spread over significant energy intervals due to the kinetic energy of the primary reactants. The secondary particle yields are typically two to three orders of magnitude lower than the primary yield, and the ratios Y_{2n}/Y_{1n}, and Y_{2p}/Y_{1n} (which are linearly dependent on ρR_{hot} in certain plasma regimes) can each be used to infer a value of ρR_{hot} for implosions of D_2-filled capsules in both direct- and indirect-drive experiments.[12-15] In those studies, the simple "hot-spot" and/or the "uniform" models were used to relate these ratios to ρR_{hot}. Although these simple models have been widely used to infer a value of ρR_{hot}, they have some serious limitations which can result in misinterpretation and errors (as described in Section II); one manifestation of these problems is often disagreement between the proton- and neutron-inferred values of ρR_{hot} calculated from experimental data (see Fig. 1). These deviations are related to a combination of mix, temperature profile, and the difference between the cross section for secondary reactions (3) and (4). These factors can cause secondary protons and neutrons to be produced in different regions of the compressed capsules (Fig. 2). In addition, other workers have noted some puzzling issues with recent secondary neutron measurements in indirect drive implosions on OMEGA.[16] In that work, the authors observed a factor-of-three larger Y_{2n}/Y_{1n} ratio and a narrower secondary neutron spectrum than predicted for these low-convergence implosions (where mix should be relatively unimportant). In contrast, for high-convergence implosions, they found better agreement between measured and predicted Y_{2n}/Y_{1n} values.

In previous work,[12] high-resolution secondary-proton spectra were obtained during experiments at the OMEGA laser facility.[17] The yields were used with measured neutron yields to estimate ρR_{hot} with the hot-spot and uniform models and it was shown that the Y_{2p}/Y_{1n} –inferred ρR_{hot} was often lower than the Y_{2n}/Y_{1n}, -inferred ρR_{hot}. This was attributed to the effects of fuel-shell mix, and it was suggested that the two inferences might be considered lower and upper limits, respectively. In this paper, that work is extended to cover a wider range of implosion types and to include Monte-Carlo simulations that allow a detailed study of the implications of more realistic models of the compressed core on the secondary production. Section II describes the hot-spot and uniform models and their limitations. Section III describes the experiments and the range of parameters that are measured. Section IV describes a Monte-Carlo program that has been developed to model the implosions to understand how particle production occurs. Results from both experiments and Monte-Carlo calculations are discussed in Section V, with an emphasis on how ρR_{hot} is related to the yields of primary and secondary particles. The results are summarized in Section VI.

II. PRIMARY AND SECONDARY PRODUCTS

The hot-spot and uniform models have been commonly used to relate Y_{2p}/Y_{1n} and Y_{2n}/Y_{1n} to ρR_{hot}. The hot-spot model assumes that an imploded capsule is a sphere of uniform density and temperature and that all primary reactions occur at the very center of the capsule. A fraction of the primary ^{3}He (tritons) fuse with thermal deuterons, producing secondary protons (neutrons) as they move radially outward. As the primary particles travel through the D plasma, they lose energy and the probability for producing secondary particles along the path varies greatly since the secondary D^{3}He and DT fusion cross sections (σ_{D3He} and σ_{DT}) are strong functions of the primary ^{3}He and T energies (Fig. 3a).[18] σ_{D3He} peaks at ~ 0.65 MeV, close to the ^{3}He birth energy (0.8 MeV), while σ_{DT} peaks at ~ 0.18 MeV, significantly lower than the triton birth energy (1.0 MeV). As a result, secondary protons are mainly produced near the ^{3}He birth position, while secondary neutrons are mainly produced further away from the triton birth position (see Fig. 3b). This information is used to calculate ρR_{hot} from Y_{2p}/Y_{1n} and Y_{2n}/Y_{1n}, and the resulting dependencies are shown in Fig. 4 for D plasmas with different temperatures and densities. The ratios each saturate at different values of ρR_{hot} for different temperatures and densities, because the primary ^{3}He and tritons generally have significantly different ranges in the plasma. If either particle stops before leaving the fuel, it will not sample the entire ρR_{hot}, and the implied value of ρR_{hot} underestimates the actual value. Y_{2p}/Y_{1n} does not depend on temperature until it starts to saturate, while Y_{2n}/Y_{1n} is sensitive to temperature well below the saturation level. Therefore, without a reasonable estimate of plasma temperature, Y_{2n}/Y_{1n} cannot be used to accurately infer ρR_{hot}.

The uniform model assumes that the primary particles are produced uniformly in a sphere of constant density and temperature. The Y_{2p}/Y_{1n} and Y_{2n}/Y_{1n} dependencies show similar behavior to the hot-spot model. The primary difference is that values of ρR_{hot} implied by the uniform model are always larger than values from the hot-spot model because the mean path length of primary particles in the D plasma is shorter by 25% in the uniform model, when saturation has not occurred. The simulations described in Section V indicate that the hot-spot model gives more meaningful values of ρR_{hot} than the uniform model. Thus, the hot-spot model will be used throughout the remainder of the paper.

Both models have limitations which can introduce errors into the analysis of ρR_{hot}. These include the saturation of Y_{2p} and Y_{2n} and the uncertainty introduced by the temperature dependence of Y_{2n}. The shapes of temperature and density profiles, and the presence of fuel-shell mix[20-22] can have substantial impact on secondary particle production. In reality, the temperature is highest and the density is lowest at the center of the implosion. As the temperature decreases and the density increases, the rate of energy loss of primary particles becomes larger. This typically causes a reduction of the secondary proton production rate and an enhancement of the secondary neutron production rate (see Fig. 3a). Fuel-shell mix lowers the temperature in the mix region, which increases the energy loss rate and results in a further reduction of the secondary proton production rate and an enhancement of the secondary neutron production rate. Shell material mixed into the fuel can directly affect secondary production by increasing the energy lost by T and ^{3}He after traveling through a given amount of D, due to the higher effective charge of the shell material mixed in.

III. EXPERIMENTS

In the direct-drive experiments described here, distributed phase plates,[23] polarization smoothing using birefringent wedges,[24] and 1-THz, two-dimensional smoothing by spectral dispersion[25] were applied to smooth the OMEGA laser beams in order to enhance implosion uniformity and the nuclear reaction rate. Three types of capsules were used to study implosions with a wide range of areal densities. Low-ρR_{hot} implosions were studied using thin (~3 μm) glass (SiO_2) shells filled with ~15 atm of D_2. Some of these capsules were irradiated with a 1-ns square pulse delivering 23 kJ of on-target energy, while others were irradiated with a shorter (600 – 800 ps) pulse with on-target energy of ~12 kJ.[26] Medium and large ρR implosions were studied using capsules with thick (~20 μm) plastic (CH) shells filled with ~15 atm of D_2, and cryogenic capsules with a ~100 μm layer of D_2 ice enclosed within a 3~5 μm thick CH shell, respectively. They were all irradiated with 1-ns square pulses, delivering 23 kJ of on-target energy.

Charged-particle data were collected with two types of spectrometers. Wedge-range-filter proton spectrometers[12,27] provided secondary-proton spectra from up to six different directions simultaneously. These spectra were used to calculate the yield and mean energy of secondary protons. Two magnet-based

charged-particle spectrometers[27] provided the spectra of primary protons and tritons for low ρR implosions. Neutron data were obtained from three diagnostics. Neutron time-of-flight detectors[28] provided primary and secondary neutron yields as well as primary-neutron-yield-averaged ion temperature ($<T_i>_{Y1n}$), and a neutron temporal diagnostic[29] measured the peak primary neutron production time and the DD burn duration. In addition, secondary-neutron spectra were obtained from the 1020-scintillator array[30] on some of the more recent implosions.

The data from each implosion then includes the five quantities, Y_{1n}, Y_{2n}, Y_{2p}, $<T_i>_{Y1n}$ and $<E_{2p}>$, which will be matched to simulations in the next section. In addition, the spectral energy distributions of the secondary protons (and sometimes secondary neutrons) will be compared with the simulations. The yields and $<T_i>_{Y1n}$, together with a realistic plasma density, can also be used to determine what the simple hot-spot and uniform models imply for values of $\rho R_{hot,2p}^{exp1}$ and $\rho R_{hot,2n}^{exp1}$ (where the superscript exp1 refers to use of the measured $<T_i>_{Y1n}$ as the characteristic ion temperature).

IV. MONTE-CARLO SIMULATIONS

A Monte-Carlo program was developed to model the experiments described in Section III. This allows us to use more realistic temperature and density profiles than those in the hot-spot and uniform models. The burn-averaged ion temperature profile [$T_i(r)$] and the shell (or cold fuel, for cryogenic capsules) density profile [$\rho_{cold}(r)$] are assumed to have super- or sub-Gaussian profiles, and the six input parameters are: T_{i0}, T_{iw}, T_{ip}, S_{r0}, S_w, and S_p characterizing the temperature and density profiles

$$T_i(r) = T_{i0} \exp[- (r/T_{iw})^{Tip}] \quad (5)$$

and

$$\rho_{cold}(r) = \rho_{cold0} \exp\{- [(r-S_{r0})/S_w]^{Sp}\}. \quad (6)$$

These parameters are varied to produce simulated particle production that best fits the measured data for each implosion. The hot-fuel density profile [$\rho_{hot}(r)$] is calculated assuming that the plasma is isobaric out to the peak shell pressure region; with this constraint ρ_{cold0} is then adjusted in order to conserve the fuel mass. (The initial fuel mass is calculated based on the initial fuel pressure and the size of the capsule.)

For computational purposes, each primary particle is assumed to produce a secondary particle, and a spectrum of particles per unit energy dN_2/dE is obtained. Since only a small fraction of the primary particles actually undergo secondary reactions, the secondary yield and spectrum need to be normalized according to $Y_2 = <P_2>Y_1$ and $dY_2/dE \approx <P_2>Y_1(dN_2/dE)/N_2$; $<P_2> \equiv <\int n_D(l)\sigma_{sec}(l)dl>$ is the probability of primary-to-secondary conversion, calculated in the program as the primary-yield-weighted mean value of

the line integral of the D number density (n_D) times the secondary fusion cross section (σ_{sec}) for all possible primary particle trajectories. The primary particle production is determined by the density and temperature profiles. The particles are followed along their trajectories through the capsule until either they escape or lose all of their energy. The probability of a secondary fusion reaction is calculated along the path of the primary particle, and then the birth position, direction, and energy of the secondary particle are calculated. The energy loss of the secondary particles is calculated to determine its contribution to a secondary spectrum. In addition to these spectra, the radial distributions of the primary and secondary particle birth positions are recorded to illustrate the effects of profiles and fuel-shell mix.

Since the model is static, the primary yield is calculated by multiplying the burn profile by the burn duration (full-width-half-maximum of the neutron production rate); therefore, the error in the measurement of the burn duration is included in the error of the primary yield. $<E_{2p}>$ is calculated from the secondary-proton spectrum, and $<T_i>_{Y1n}$ is determined in the region where the primary particles are produced.[31] Each of the six input parameters is varied over a large range, initially using large steps to identify the region of small χ^2. This region is then more carefully explored using finer grids; as a result, the six-dimensional parameter space is explored completely. For each set of model parameters, the predicted values of the experimentally-measured quantities are calculated and the quality of agreement with the data from a particular implosion is characterized with the total χ^2, which takes account of uncertainties in the experimental measurements. For each implosion, it is found that multiple local minima exist within the space of model parameters but that there is one clear region with the smallest values of χ^2. Errors on the values of individual model parameters are then estimated by asking how much they can be changed without causing the total χ^2 to increase by more than one. Although the widths and shapes of secondary-proton spectra are not used as fit criteria, it will be seen that the predicted spectra match the measured spectra quite well; this fact provides extra confidence that the best-fit model parameters are realistic.

The characteristics of the best-fit model for each implosion were used to determine how realistic the hot-spot-model inferred values of ρR_{hot} are. Values of Y_{2p}/Y_{1n}, Y_{2n}/Y_{1n}, $<T_i>_{Y1n}$ and plasma density from the simulations were used to infer $\rho R_{hot,2p}^{sim1}$ and $\rho R_{hot,2n}^{sim1}$ according to Fig. 4 (the superscript sim1 indicates that $<T_i>_{Y1n}$ was used as the characteristic ion temperature). The values of $\rho R_{hot,2p}^{sim2}$ and $\rho R_{hot,2n}^{sim2}$ were calculated assuming that the appropriate temperatures are averages weighted by secondary yields ($<T_i>_{Y2p}$ and $<T_i>_{Y2n}$, respectively). These values were then compared with $\rho R_{hot}^{int} \equiv \int \rho_D dr$, integrated over the hot-fuel region.

V. RESULTS

A. Low areal density implosions

For low-ρR_{hot} implosions, the primary ^{3}He and T traverse the entire hot-fuel region, and the values of ρR_{hot} inferred from secondary protons and neutrons using the hot-spot (or uniform) model generally agree with each other and usually give a reasonable estimate of the actual value of ρR_{hot}. This is shown experimentally by the square points in Fig. 1, which compares values of $\rho R_{hot,2p}^{exp1}$ and $\rho R_{hot,2n}^{exp1}$. These values were inferred according to Fig. 4 assuming a D plasma with a a temperature of $<T_i>_{Y1n}$ keV and a density of 1.5 g/cc (obtained from a typical best-fit simulation, as discussed below). Fig. 1 also illustrates that $\rho R_{hot,2p}^{exp1}$ and $\rho R_{hot,2n}^{exp1}$ are larger for implosions with lower (~12 kJ) on-target laser energy (open squares) than for implosions with full (~23 kJ) laser energy (closed squares). This could be explained by a larger amount of glass shell being ablated away in full energy implosions, resulting in less material to drive the fuel inward.[32,33] (Fig. A.1). In addition, these values of ρR_{hot}^{exp1} from D_2 implosions with full laser energy show reasonable agreement with values from similar thin-glass shell DT implosions,[34,12] for which the knock-on method[35] was used to determine the ρR_{hot}.

For implosion 30981, which involved a 3.1 μm glass shell filled with 14.7 atm of D_2 gas, Fig. 5a shows simulated density and temperature profiles from the best-fit simulation. Fig. 5b shows radial distributions of the primary and secondary particle birth positions; secondary protons and neutrons are produced in virtually identical regions of the capsule. In addition, a high plasma temperature and a low ρR_{hot} result in similar values of ρR_{hot}^{sim1} inferred from the simulated secondary yields. Values of ρR_{hot}^{sim1} are inferred using the hot-spot model and assuming a plasma temperature of $<T_i>_{Y1n}$ keV and a plasma density of 1.5 g/cc (obtained from simulation). In addition, values of ρR_{hot}^{sim1} agree with ρR_{hot}^{int} obtained from the fuel density profile shown in Fig. 5a; this indicates that the small amount of fuel-shell mix in this type of implosion does not have much impact on the accuracy of the simple model. Results of the simulation along with measured data are summarized in Table I.

Simulated secondary spectra are in good agreement with measured spectra as shown in Figs. 5c and 5d. The measured secondary proton spectrum is an average of five spectra obtained simultaneously at different angles from implosion 30981.

B. Medium areal density implosions

Correctly inferring the value of ρR_{hot} is more difficult for implosions of capsules with thick plastic shells because Y_{2p} reaches saturation when ρR_{hot} is sufficiently large, and Y_{2n} is enhanced in the presence of increased fuel-shell mix. The triangles in Fig. 1 show that the values of $\rho R_{hot,2p}^{exp1}$ are often

smaller than values of $\rho R_{hot,2n}^{exp1}$, as previously reported in Ref. 12. Values of $\rho R_{hot,2p}^{exp1}$ and $\rho R_{hot,2n}^{exp1}$ are inferred assuming a temperature of $<T_i>_{Y1n}$ keV and a D plasma with a density of 2 g/cc.

Fig. 6a shows the temperature and density profiles that result in the best fit to the measured data for implosion 27443 (19.4 μm plastic shell filled with 15 atm of D_2 gas), and Fig. 6b shows the resulting radial distributions of primary and secondary particle birth positions. About 32 % of the initial CH mass remains, and ~ 1.3 μm of the initial CH layer has mixed into the fuel (which is similar to the amount of mix reported in Refs. 20-22.[36] The ^{3}He are ranged out before traversing the entire fuel region. Fig. 6b also illustrates an enhancement of Y_{2n} by fuel-shell mix; the increased energy loss of T per unit ρR_{hot}, due to the cooler, dense shell material, results in an enhanced DT fusion cross section (Fig. 3), which causes Y_{2n}/Y_{1n} to overestimate ρR_{hot}^{int}. In addition, Y_{2n}/Y_{1n} is more sensitive to temperature in this ρR_{hot} range; using $<T_i>_{Y1n}$, which is always higher than $<T_i>_{Y2n}$, results in a larger inferred value of ρR_{hot}.

Simulated yields and additional parameters characterizing the implosion are summarized and compared with measurements in Table II. This table shows that the values of ρR_{hot}^{sim1} implied by secondary protons and neutrons are smaller and larger than the value of ρR_{hot}^{int}, respectively. The hot-spot model was used to obtain values of ρR_{hot} using $<T_i>_{Y1n}$ keV for the temperature and assuming the density of the D plasma was 2 g/cc.

The simulated secondary proton spectrum is compared with the measured spectrum in Fig. 6c. The measured secondary proton spectrum is an average of three spectra simultaneously obtained at different angles from implosion 27443, and shows more downshift than spectra from the low ρR_{hot} implosions. The widths of the secondary proton and neutron spectra (Fig. 6d) are slightly narrower than in the previous case because the average energy of the primary particle, at the time it undergoes secondary fusion, is smaller.[12]

C. Cryogenic implosions

For cryogenic implosions, the interpretation of inferred values of ρR_{hot} is even more subtle, since there is a high-temperature, low-density fuel region and a low-temperature, high-density fuel region. If most of the secondary particles are produced only in the hot-fuel region, then Y_2/Y_{1n} can be used to infer ρR_{hot}. On the other hand, if secondary particles are mainly produced in the inner part of the cold fuel region, the inferred ρR is larger than ρR_{hot}, but smaller than ρR_{total}. (Even the more penetrating T cannot traverse the entire cold fuel region since the range of T in a 8 g/cc, 1 keV D plasma is ~ 15 mg/cm^2, and we usually calculate ρR_{total} > 40 mg/cm^2 from the downshift of the average secondary proton energy for cryogenic implosions). Fig. 1 shows that values of ρR_{hot} implied by measured Y_{2n}/Y_{1n} are always larger

than values from measured Y_{2p}/Y_{1n} for those implosions (values were inferred assuming a $<T_i>_{Y1n}$ keV, 3 g/cc D plasma).

Radial profiles of temperature and density calculated for implosion 28900 (89-μm D_2 ice layer inside of 5.1-μm CH shell) are shown in Fig. 7a, and simulated and measured spectra are shown in Figs. 7c and 7d. As indicated in Fig. 7d, the secondary-neutron spectrum is much narrower than the secondary-neutron spectra from Figs. 5d and 6d (Fig. A.2) because the primary T are, on average, less energetic when they fuse with thermal D.[12] Measurements of secondary-neutron spectra from more recent cryogenic implosions also show the same characteristics.

The radial distributions of the primary and secondary birth positions shown in Fig. 7b indicate that secondary protons and neutrons are born mainly in the hot and cold fuel regions, respectively. Therefore, the ρR obtained from secondary protons gives an estimate of ρR_{hot}, while the secondary neutron yield provides a lower limit on ρR_{total}. In this type of implosion, effects of mix or exchange of hot and cold fuel play significant roles in determining the radial distribution of secondary birth positions.

Simulated values of yields and other important implosion characteristics are compared with experimental results in Table III. The secondary-neutron, hot-spot-model-inferred ρR^{sim1} is close to $\rho R_{total}{}^{int}$, but this does not mean that the hot-spot model describes the implosion accurately. The agreement is an accidental consequence of using the wrong temperature, $<T_i>_{Y1n}$, which samples the hotter central region rather than the cooler fuel region where most of the secondary neutrons are produced.

This implosion has also been analyzed using a combination of x-ray and neutron measurements, without the use of secondary proton data. These results are discussed in Ref. 37. While the best-fit profiles were somewhat different, they agree within the uncertainties of the two simulation techniques.

VI. CONCLUSIONS

The hot-spot and uniform models have been used to infer the areal density of the hot-fuel region (ρR_{hot}) of D_2 implosions, but disagreements between the values of ρR_{hot} inferred from secondary proton and neutron yields have often been observed, indicating limitations in these models. Results from direct-drive experiments at the OMEGA laser system and Monte-Carlo simulations provided a deeper understanding of the relationship between ρR, the capsule structure, and secondary particle production. Experiments show that values of ρR_{hot} inferred from the ratios of secondary proton and neutron to primary neutron yields (Y_{2p}/Y_{1n} and Y_{2n}/Y_{1n}) using the hot-spot model agree well for low ρR_{hot} implosions (thin-glass shell capsules), and simulations indicate that they give a good estimate of the actual value of ρR_{hot}. The results from implosions of D_2-filled thin-glass shells also show reasonably good agreement with results from implosions of similar capsules filled with DT gas. For thick-plastic-shell

capsule implosions, where the ρR_{hot} of an implosion becomes sufficiently large, Y_{2p}/Y_{1n} underestimates ρR_{hot} since the primary ^{3}He are ranged out before sampling the entire hot-fuel region. In addition, fuel-shell mix increases the rate of energy loss of ^{3}He and causes Y_{2p}/Y_{1n} to further underestimate ρR_{hot}. The fuel-shell mix also causes Y_{2n}/Y_{1n} to overestimate ρR_{hot} by slowing down the primary T, thereby increasing the secondary DT fusion reaction cross section. As a result, values of ρR_{hot} for medium ρR_{hot} capsules inferred from Y_{2p}/Y_{1n} and Y_{2n}/Y_{1n} using the hot-spot model should be interpreted as estimates of the lower and upper limits on the actual ρR_{hot}, respectively. For cryogenic capsules, secondary protons are produced mainly in the hot-fuel region, and the proton-implied value of ρR provides a good estimate of the hot-fuel ρR. In contrast, secondary neutrons are mostly produced in the inner part of the cold fuel region, and the neutron-implied ρR gives a lower limit on the total ρR when calculated correctly using the secondary-neutron-birth-point average temperature and density. Naive use of the simple hot-spot or uniform model, with a burn-averaged temperature, often results in inaccurate inference of ρR_{hot}. More thorough analysis, such as the use of complete data sets and simulations for determining the secondary birth positions and the effects of mix, as presented herein, or the use of detailed analysis of secondary neutron spectra both from experiments and simulations[10], is required in order to obtain a realistic estimate of ρR_{hot}.

ACKNOWLEDGMENTS

This work described here was performed in part at the LLE National Laser Users' Facility (NLUF), and was supported in part by the US DoE (grant DE-FG03-03SF22691), US DoE DP/NNSA (Cooperative Agreement DE-FG03-03NA00058), LLE (subcontract 412160-001G), and LLNL (subcontract B504974).

References

[1]S. W. Haan, S. Pollanine, J. D. Lindl *et al.*, Phys. Plasmas **2**, 2480 (1995).

[2]J. D. Lindl, R. L. McCrory, and E. M. Campbell, Phys. Today **45**, 32 (1992).

[3]J. D. Lindl, Phys. Plasmas **2**, 3933 (1995).

[4]H. D. Campbell and F. H. Southworth, in *Proceedings of the First Topical Meeting on the Technology of Controlled Nuclear Fusion* (American Nuclear Society, LaGrange Park, IL, 1974), p. 75.

[5]E. G. Gamalii, S. Yu, Gus'kov, O. N. Krokhin, and V. B. Rusanov, JETP Lett. **21,** 70 (1975).

[6]S. Skupsky and S. Kacenjar, J. Appl. Phys. **52,** 2608 (1981).

[7]T. E. Blue and D. B. Harris, Nucl. Sci. Eng. **77,** 463 (1981).

[8]T. E. Blue, J. W. Blue, J. S. Durham, D. B. Harris, A. S. Hnesh, and J. J. Reyes, J. Appl. Phys. **54,** 615 (1983).

[9]H. Azechi, N. Miyanaga, R. O. Stapf *et al.*, Appl. Phys. Lett. **49,** 555 (1986).

[10]M. D. Cable and S. P. Hatchett, J. Appl. Phys. **62,** 2233 (1987).

[11]H. Azechi, M. D. Cable, and R O. Stapf, Laser Part. Beams **9,** 119 (1991).

[12]F. H. Séguin, C. K. Li, J. A. Frenje *et al.*, Phys. Plasmas **9,** 2725 (2002).

[13]Peter Amendt, R. E. Turner, and O. L. Landen, Phys. Rev. Lett. **89,** 165001 (2002).

[14]T. C. Sangster, J. A. Delettrez, R. Epstein *et al.*, Phys. Plasmas **10,** 1937 (2003).

[15]C. Stoeckl, C. Chiritescu, J. A. Delettrez *et al.*, Phys. Plasmas **9,** 2195 (2002).

[16]R. E. Turner, P. A. Amendt, O. L. Landen *et al.*, Bull. Am. Phys. Soc. 47, 328 (2002).

[17]T. R. Boehly, D. L. Brown, R. S. Craxton *et al.*, Opt. Commun. **133**, 495 (1997).

[18]S. Glasstone and R. H. Lovberg, *Controlled Thermonuclear Reactions: An Introduction to Theory and Experiment* (Van Nostrand, Princeton, NJ, 1960).

[19]C. K. Li and R. D. Petrasso, Phys. Rev. Lett. **70,** 3059 (1993).

[20]P. B. Radha, J. Delettrez, R. Epstein *et al.*, Phys. Plasmas **9,** 2208 (2002).

[21]C. K. Li, F. H. Séguin, J. A. Frenje *et al.*, Phys. Rev. Lett. **89,** 165002 (2002).

[22]S. P. Regan, J. A. Delettrez, F. J. Marshall *et al.*, Phys. Rev. Lett. **89**, 085003 (2002).

[23]Y. Lin, T. J. Kessler, and G. N. Lawrence, Opt. Lett. **20**, 764 (1995).

[24]T. R. Boehly, V. A. Smalyuk, D. D. Meyerhofer *et al.*, J. Appl. Phys. **85**, 3444 (1999).

[25]S. Skupsky, R. W. Short, T. Kessler *et al.*, J. Appl. Phys. **66**, 3456 (1989).

[26]Short laser pulses (< 1 ns) imploding thin-glass shell capsules prevent significant nuclear production while the laser is on. This is important if ρR_{total} is to be studied, because the capsule can be charged to a significant potential relative to the target chamber wall due to laser-plasma interactions. The potential can cause an upshift of measured proton energies,[35,38,39] making it difficult to determine how much energy the protons lost while leaving the capsule (necessary for calculating ρR_{total}). The potential decays away

rapidly after the laser is turned off, so it does not affect measurements of protons from implosions in which the nuclear burn occurs after the pulse (such as those involving thick-plastic-shell or cryogenic capsules[35]). This affects only the study of ρR_{total}; measurements of yields are unaffected by capsule potentials.

[27]F. H. Séguin, J. A. Frenje, C. K. Li *et al.*, Rev. Sci. Instrum. **74,** 975 (2003).

[28]M. A. Russotto and R. L. Kremens, Rev. Sci. Instrum. **61,** 3125 (1990).

[29]R. A. Lerche, D. W. Phillion, and G. L. Tietbohl, Rev. Sci. Instrum. **66**, 933 (1995).

[30]V. Yu. Glebov, C. Stoeckl, S. Roberts *et al.*, Bull. Am. Phys. Soc. 48, 342 (2003).

[31]Primary-neutron-yield-weighted-average ion temperature is calculated by two methods, each yielding a virtually identical temperature. First, the product of the temperature and the primary neutron birth rate per unit length at each radius is integrated and divided by the primary neutron yield. Second, the primary neutron spectrum is calculated, and the width of the spectrum was used to obtain an ion temperature.

[32]J. D. Lindl, *Inertial Confinement Fusion* (Springer-Verlag, New York, 1998).

[33]M. D. Rosen and J. H. Nuckolls, Phys. Fluids 22, 1393 (1979).

[34]M. J. Canavan, *et al.*, to be submitted to Rev. Sci. Instrum. (2004); herein the laser energy was ~30 kJ for these DT implosions.

[35]C. K. Li, F. H. Séguin, D. G. Hicks *et al.*, Phys. Plasmas **8**, 4902 (2001).

[36]Radha *et al.*,[20] Li *et al.*,[21] and Regan *et al.*[22] reported ~ 1 μm, ~ 0.5 μm, and ~ 0.4 μm of the initial shell layer mixed into the fuel, respectively.

[37]V. A. Smalyuk, J. A. Dellettrez, S. B. Dumanis *et al.*, "Hot-Core Characterization of the Cryogenic D_2 Target at Peak Neutron Production in Direct-Drive Spherical Implosion," submitted to Phys. Rev. Lett.

[38]D. G. Hicks, C. K. Li, F. H. Séguin *et al.*, Phys. Plasmas **8,** 606 (2001).

[39]D. G. Hicks, C. K. Li, F. H. Séguin *et al.*, Phys. Plasmas **7,** 5106 (2000).

Table I. Measured and simulated values of yields and ρR for OMEGA implosion 30981. Experimental data were fitted by adjusting ρ(r) and T_i(r). Total χ^2 along with parameters specifying the cold (SiO_2) temperature and density Gaussian profiles [peak temperature (T_{i0}), 1/e radius (T_{iw}), power of the exponent (T_{ip}), peak density radius (S_{r0}), 1/e radius (S_w), and power of the exponent (S_p)] are also listed. $\rho R_{cold} = \int \rho_{cold} dr$, integrated radially over the SiO_2 shell region, and $\rho R_{hot} = \int \rho_D dr$ integrated radially over the hot-fuel region of the simulated profiles. Values of $\rho R_{hot,\ 2n}$ and $\rho R_{hot,\ 2p}$ were deduced using measured (left column) and simulated (right column) yield ratios assuming a 1.5 +/- 1 g/cc (obtained from Fig. 5a) D plasma at $<T_i>_{Y1n}$ +/- 0.5 keV.

Shot 30981

	Measured	Simulated
Y_{1n}	(1.5 +/- 0.15) E+11	(1.5 +0.23 –0.18) E+11
Y_{2n}/Y_{1n}	(5.1 +/- 0.98) E-4	(5.1 +1.1 –0.57) E-4
Y_{2p}/Y_{1n}	(7.9 +/- 1.1) E-4	(7.6 +1.0 –0.96) E-4
$<E_{2p}>$ (MeV)	14.47 +/- 0.1	14.64 +0.14 –0.16
$<T_i>_{Y1n}$ (keV)	8.2 +/- 0.5	8.2 +0.7 –0.5
χ^2	…	0.1
T_{i0} (keV)	…	20.5 +2.5 –10
T_{iw} (μm)	…	34 +14 –4
T_{ip}	…	2 +5 –0
S_{r0} (μm)	…	62 +6 –10
S_w (μm)	…	3.5 +3 –3.3
S_p	…	2.5 +≥7.5 –2
ρR_{cold} (mg/cm^2)	…	4.5 +4.3 –4.2
ρR_{hot} (mg/cm^2)	…	3.7 +0.8 –0.4
$\rho R_{hot,2n}$ (mg/cm^2)	4.6 +0.9 – 1.2	4.6 +1.0 –0.6
$\rho R_{hot,2p}$ (mg/cm^2)	4.3 +0.6 – 0.8	4.1 +/- 0.5

Table II. Measured and calculated values of implosion characteristics for OMEGA implosion 27443. Values ρR_{hot} were calculated assuming a 2 +/- 1 g/cc D plasma at $\langle T_i \rangle_{Y1n}$ +/- 0.5 keV. Results from simulation (right column) indicate that the $\rho R_{hot,2p}$ underestimates and $\rho R_{hot,2n}$ overestimates the actual value.

Shot 27443

	Measured	Simulated
Y_{1n}	(1.5 +/- 0.15) E+11	(1.6 +0.1 –0.25) E+11
Y_{2n}/Y_{1n}	(1.5 +/- 0.24) E-3	(1.4 +0.16 –0.12) E-3
Y_{2p}/Y_{1n}	(1.0 +/- 0.14) E-3	(1.0 +0.1 –0.15) E-3
$\langle E_{2p} \rangle$ (MeV)	13.1 +/- 0.1	13.07 +0.1 –0.11
$\langle T_i \rangle_{Y1n}$ (keV)	4.1 +/- 0.5	4.1 +0.2 –0.4
χ^2	…	0.5
T_{i0} (keV)	…	11 +0 –5.5
T_{iw} (μm)	…	20 +18 -0
T_{ip}	…	0.8 +1.2 -0
S_{r0} (μm)	…	54 +/- 2
S_w (μm)	…	16 +2 –6
S_p	…	1.2 +0 –0.2
ρR_{cold} (mg/cm^2)	…	42.3+3.9 –2.1
ρR_{hot} (mg/cm^2)	…	8.9 +1 –0.4
$\rho R_{hot,2n}$ (mg/cm^2)	12.8 +/- 1.9	11.6 +1.2 -1
$\rho R_{hot,2p}$ (mg/cm^2)	5.0 +/- 0.7	5.2 +0.5 –0.7

Table III. Measured and calculated values of implosion characteristics for OMEGA implosion 28900. $\rho R_{total} = \int \rho_D dr$, integrated radially over the entire simulated profiles. ρR_{hot} is defined as the ρR that includes 90% of primary production. Values of ρR_{hot} were calculated assuming a 3.0 +/- 1.5 g/cc D plasma at $<T_i>_{Y1n}$ +/- 0.5 keV. Results from the simulation (right column) suggest that value of $\rho R_{hot,2p}$ provides a good estimate of ρR_{hot}. Secondary neutron implied ρR_{hot} is similar to ρR_{total}, but this is because the value of the temperature used to infer ρR_{hot} is too large. If the temperature of the cold fuel region (1 keV instead of 3.6 keV) were used, a much smaller and physical value of ρR_{hot} would be implied.

Shot 28900

	Measured	Simulated
Y_{1n}	(1.2 +/- 0.12) E+11	(1.3 +0.12 –0.14) E+11
Y_{2n}/Y_{1n}	(9.4 +/- 1.4) E-3	(9.1 +1.0 –1.1) E-3
Y_{2p}/Y_{1n}	(1.8 +/- 0.26) E-3	(1.6 +0.0 –0.2) E-3
$<E_{2p}>$ (MeV)	13.31 +/- 0.10	13.28 +0.15 –0.11
$<T_i>_{Y1n}$ (keV)	3.6 +/- 0.5	3.5 +0.6 -0.3
χ^2	...	0.6
T_{i0} (keV)	...	8.5 +9.5 –2.5
T_{iw} (μm)	...	18 +10 –8
T_{ip}	...	1.2 +0.6 -0.4
S_{r0} (μm)	...	52 +22 –2
S_w (μm)	...	32 +16 –12
S_p	...	9 +≥1 –7.5
ρR_{total} (mg/cm^2)	...	48.2 +3.2 -6.0
ρR_{hot} (mg/cm^2)	...	7.9 +0.2 –1.7
$\rho R_{hot,2n}$ (mg/cm^2)	49.8 +5.0 –6.9	48.0 +4.9 –4.0
$\rho R_{hot,2p}$ (mg/cm^2)	9.3 +1.9 –1.5	7.8 +0.5 –0.6

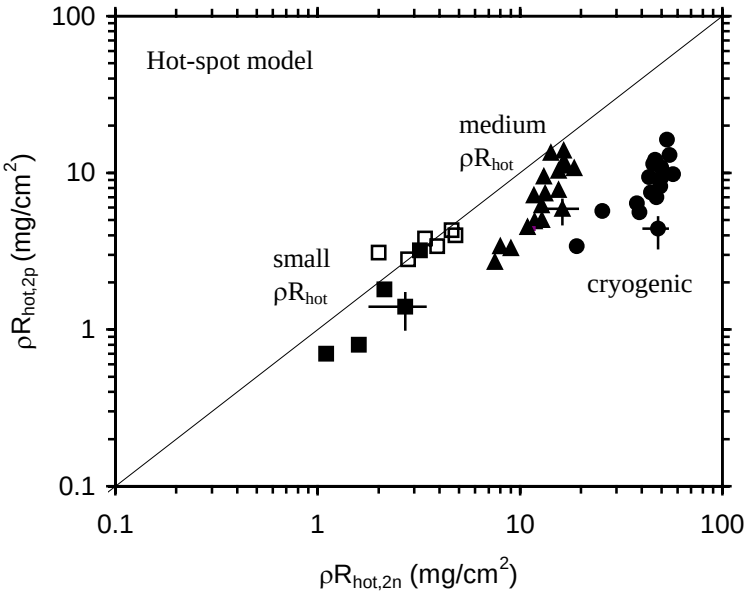

FIG. 1. Secondary proton- and neutron-implied values of ρR_{hot} are compared for implosions of small ρR_{hot} (squares), medium ρR_{hot} (triangles), and cryogenic (circles) capsules at the OMEGA laser facility. For small ρR_{hot} implosions, the values of ρR_{hot} inferred from secondary protons and neutrons using the simple hot-spot model agree well. It is also shown that values of ρR_{hot} are larger for implosions with ~12-kJ laser energy (open squares) than for implosions with ~23-kJ laser energy (closed squares) (Fig. A.1). For these dramatically overdriven implosions, it is possible that the effects of mix are coming back into play, as indicated by the observation that $\rho R_{hot,2n}$ is larger than $\rho R_{hot,2p}$. However, for implosions with larger ρR_{hot}, the values inferred from secondary neutrons are always larger than the values from secondary protons. The error bars shown are typical of each type of implosion; they include uncertainties in the measurements and in the assumed values of the density.

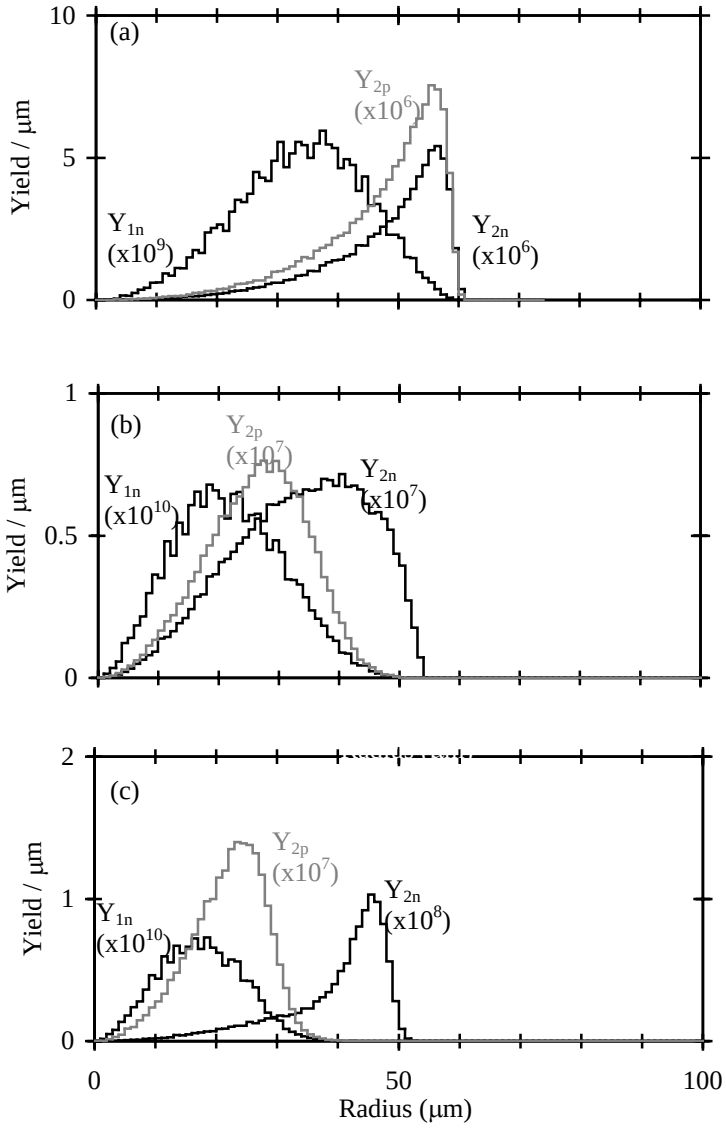

FIG. 2. Calculated radial distributions of primary and secondary birth positions per unit length for (a) low ρR implosion 30981, (b) medium ρR implosion 27443, and cryogenic implosion 28900. For low ρR implosions, where ρR_{2p} and ρR_{2n} agree reasonably well, birth positions of secondary protons and neutrons are virtually identical. However, for medium ρR and cryogenic implosions, where ρR_{2n} is always larger than ρR_{2p}, secondary neutrons are produced in more outer regions compared to secondary protons. Note that calculated radial distributions of primary birth rates per unit volume (as opposed to unit radius) are shown in FIGs. A.3, A.4, and A.5 for these three implosions.

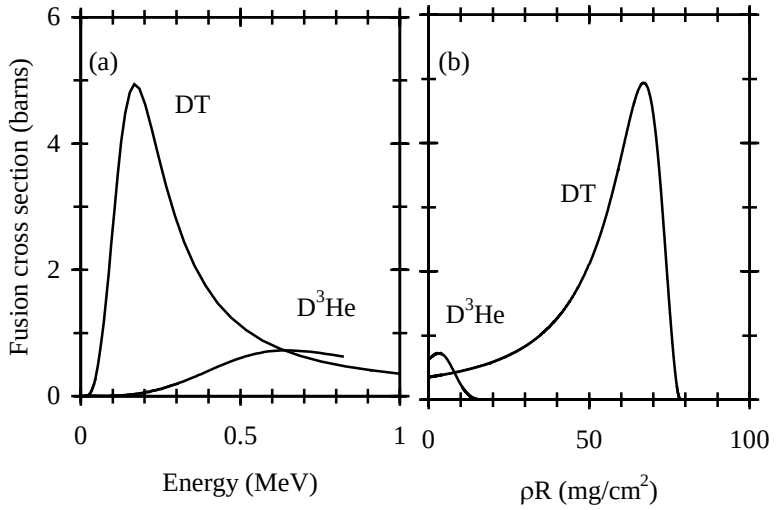

FIG. 3. (a) Dependence of the secondary D^3He (DT) reaction cross section on the energy of the primary ^3He (T) in a cold D plasma.[18] The D^3He reaction cross section is peaked close to the birth energy of ^3He, while the DT reaction cross section peaks dramatically after T has lost most of its energy. (b) As a result, secondary protons are created close to the birth points of primary ^3He (here defined as $\rho R=0$) while secondary neutrons are produced away from the birth points of primary T ($\rho R=0$). Although this plot is for a 1g/cc, 3keV D plasma, it looks similar for plasmas with different densities and temperatures.

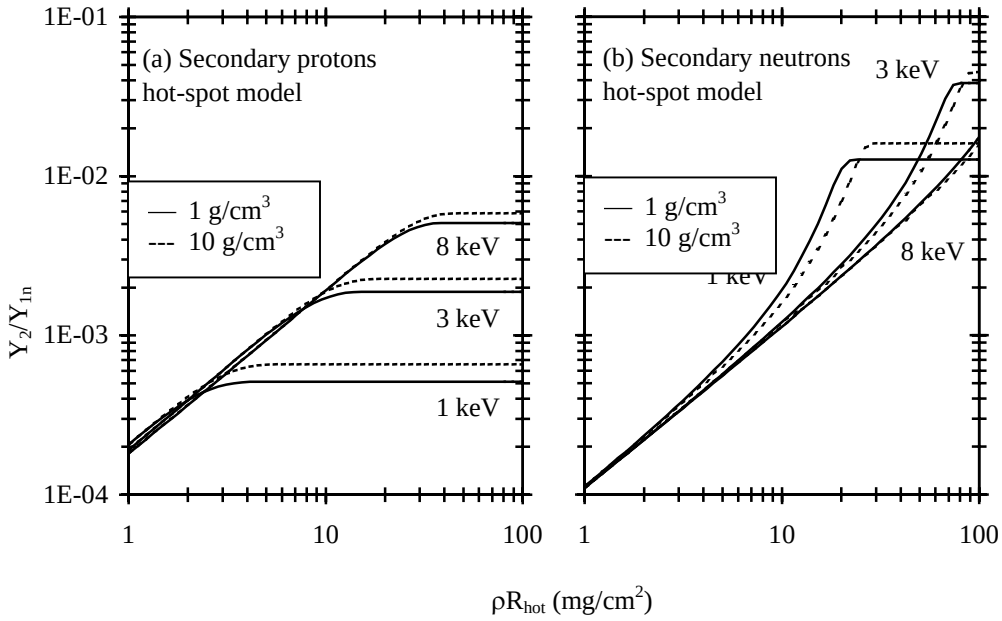

FIG. 4. (a) Y_{2p}/Y_{1n} and (b) Y_{2n}/Y_{1n} as functions of ρR_{hot} for a 1, 3, and 8 keV D plasma of 1 g/cc (solid line) and 10 g/cc (dashed line) using the hot-spot model. The energy losses of primary ^{3}He and T were calculated according to Ref. 19, and the fusion cross sections were calculated according to Ref. 18. Y_{2p}/Y_{1n} is temperature independent until it reaches the saturation levels. In contrast, Y_{2n}/Y_{1n} is temperature dependent well below saturation levels.

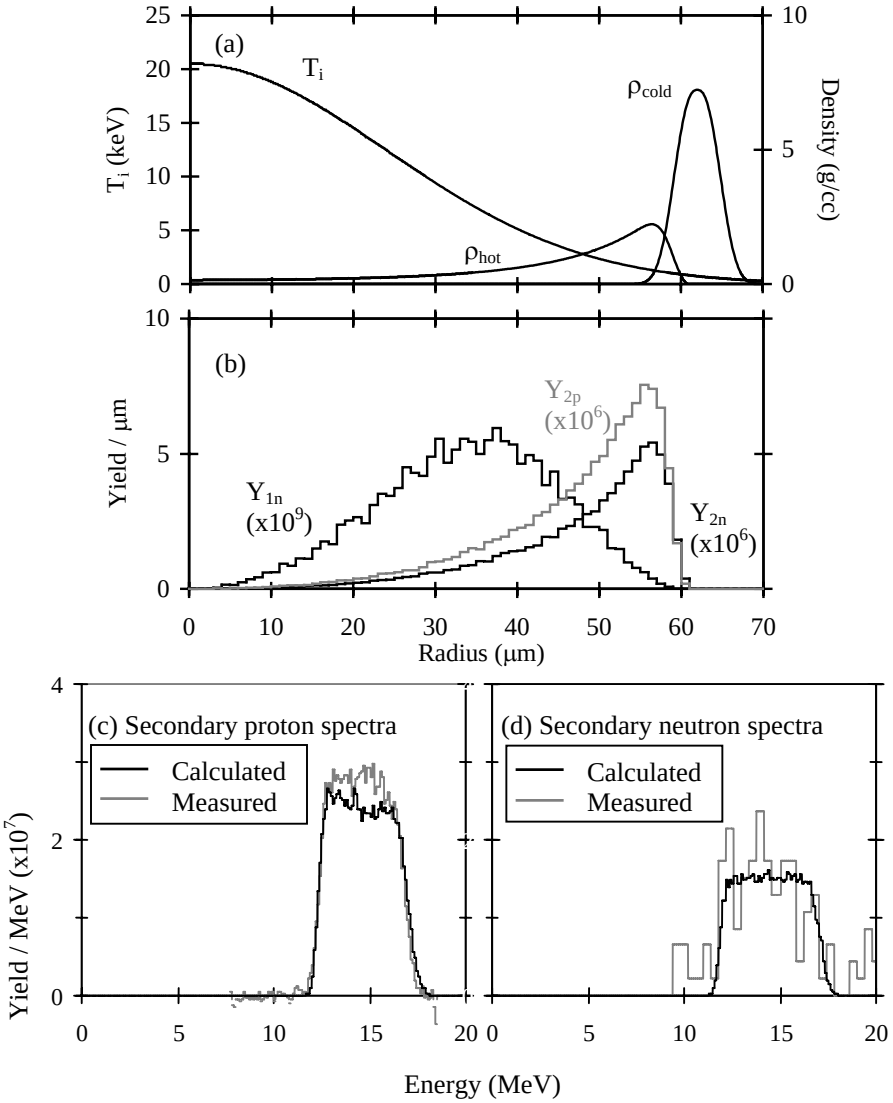

FIG. 5. Parameters from the best-fit Monte-Carlo simulation of shot 30981 (3.1 μm SiO_2 shell filled with 14.7 atm D_2). (a) $T_i(r)$ and $\rho(r)$. Fuel mass is fully conserved, while 11 % of the shell mass remains. (b) Radial distributions of the birth positions of primary and secondary particles indicate that secondary protons and neutrons are produced in a virtually identical region of the capsule. (c) Measured and simulated secondary-proton and (d) secondary-neutron spectra. Note that the shape and width of the simulated proton spectrum are very similar to those of the measured spectrum, even though these were not part of the fitting procedure. The difference in calculated and measured secondary yields are within the measurement uncertainties. Measured and simulated values of implosion characteristics are summarized in Table I. Fig. A.3 indicates how the radial profiles of T_i and ρ can change without changing the quality of the fit to the data too much.

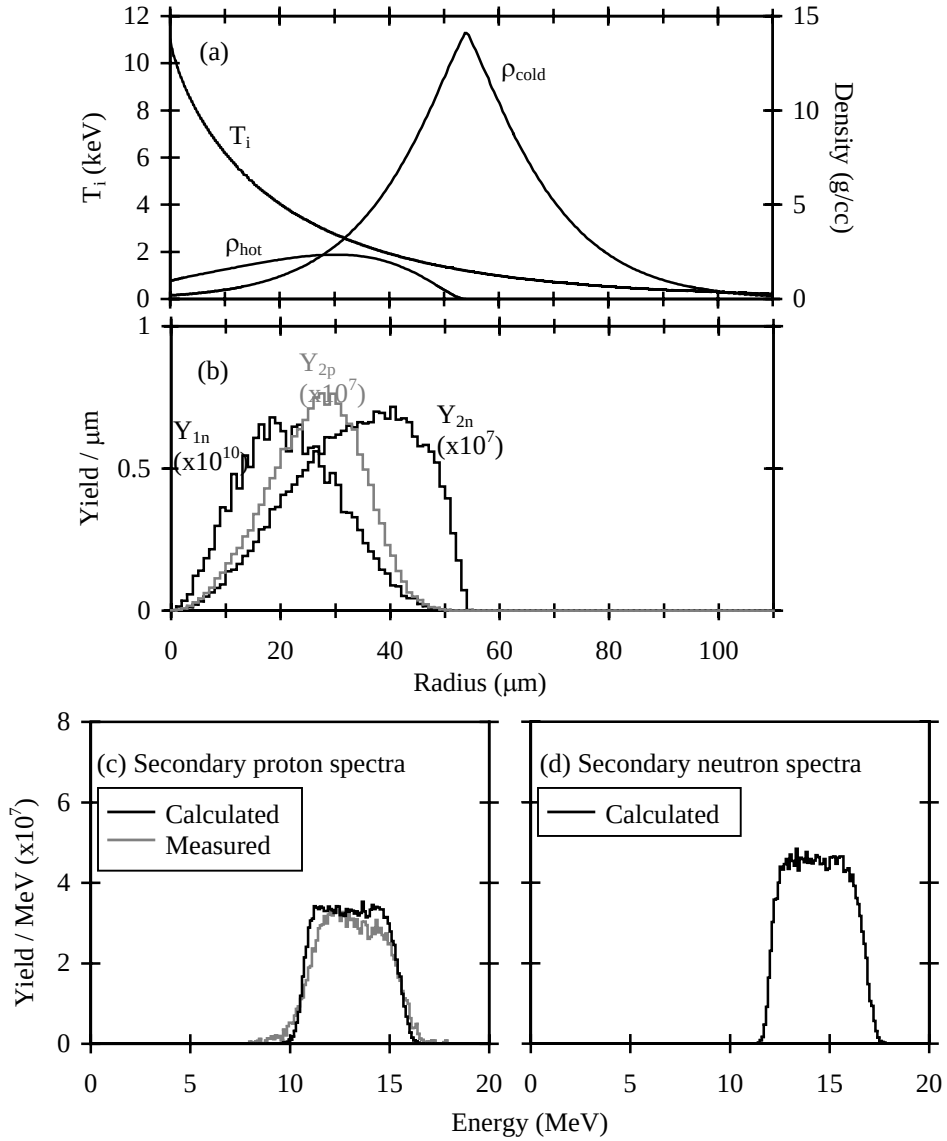

FIG. 6. Best-fit parameters from the Monte-Carlo simulation for shot 27443, which involved a 19.4 μm CH shell filled with 15 atm D_2. (a) $T_i(r)$ and $\rho(r)$. Fuel mass is fully conserved, while 32 % of the shell mass remains. (b) Radial distributions of the birth positions of primary and secondary particles show that secondary proton production is diminished, while secondary neutron production is enhanced in the region of significant fuel-shell mix. This causes secondary protons to underestimate, and secondary neutrons to overestimate the actual value of ρR_{hot}. (c) Measured and simulated secondary proton spectra are compared, and (d) simulated secondary neutron spectrum is shown. The secondary proton spectra show more energy downshift, and the width of the secondary spectra are slightly narrower, than the low ρR_{hot} case because the average primary particle energy is smaller at the time of secondary reaction. Experimental and simulated values of implosion characteristics are listed in Table II, while other fits are illustrated in Fig. A.4.

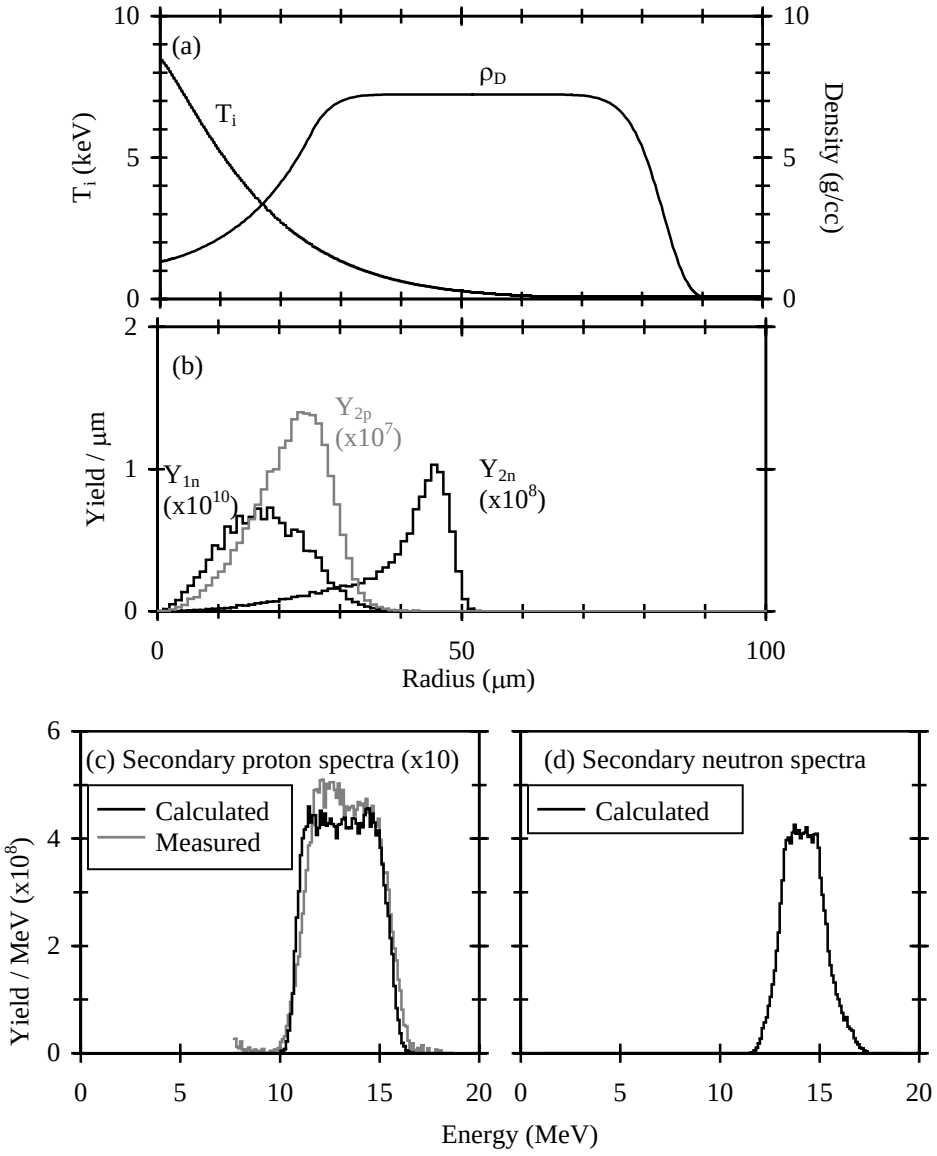

FIG. 7. (a) Simulated profile of shot 28900 (cryogenic capsule with a 5.1 μm CD shell and 89 μm D_2 ice layer) which gives the best fit to the measurement. 31 % of the total mass remains. (b) Radial distributions of the birth points of primary and secondary particles show that most of the secondary protons are produced in the hot-fuel region, while secondary neutrons are mainly produced in the cold fuel region. (c) Measured and simulated secondary proton spectra. (d) Simulated secondary neutron spectrum is narrower than the spectra in Figs. 5d and 6d because primary T are less energetic at the time they undergo secondary reactions; ρR of cold fuel is large enough to stop primary T (Fig. 7.b), and the cross section increases as T loses energy (Fig. 3a). Important implosion characteristics are summarized in Table III, while other fits are illustrated in Fig. A.5.

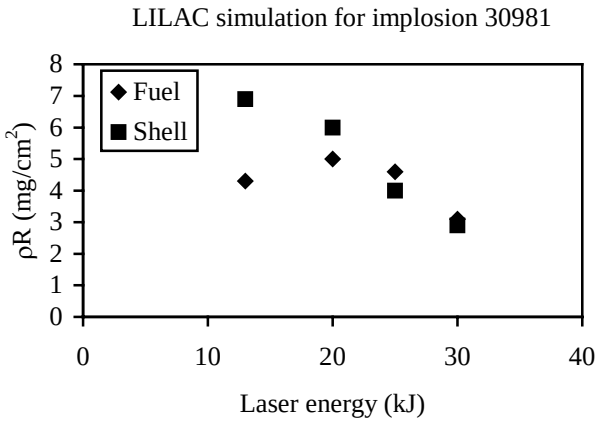

FIG. A.1. 1D clean LILAC simulations for low ρR implosion 30981 indicate hot-fuel ρR starts to decrease as the capsule is significantly overdriven. This trend agrees with measurements where ρR_{hot} are lower for full-laser energy (~23 kJ) driven thin-glass shell capusles than for low laser energy (~12 kJ) driven capsules (Fig. 1).

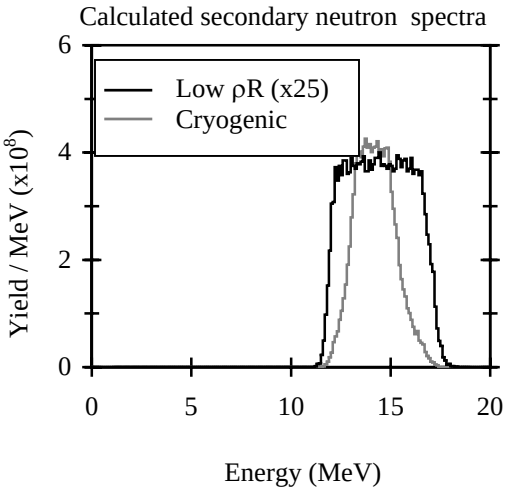

FIG. A.2. The simulated secondary neutron spectrum is narrower than the spectra in Figs. 5d and 6d because the primary T are less energetic at the time they undergo secondary reactions; ρR of cold fuel is large enough to stop primary T (Fig. 7.b), and the cross section increases as T loses energy (Fig. 3a). Note that detailed analysis of secondary neutron spectra was used to study areal density in Ref. 10.

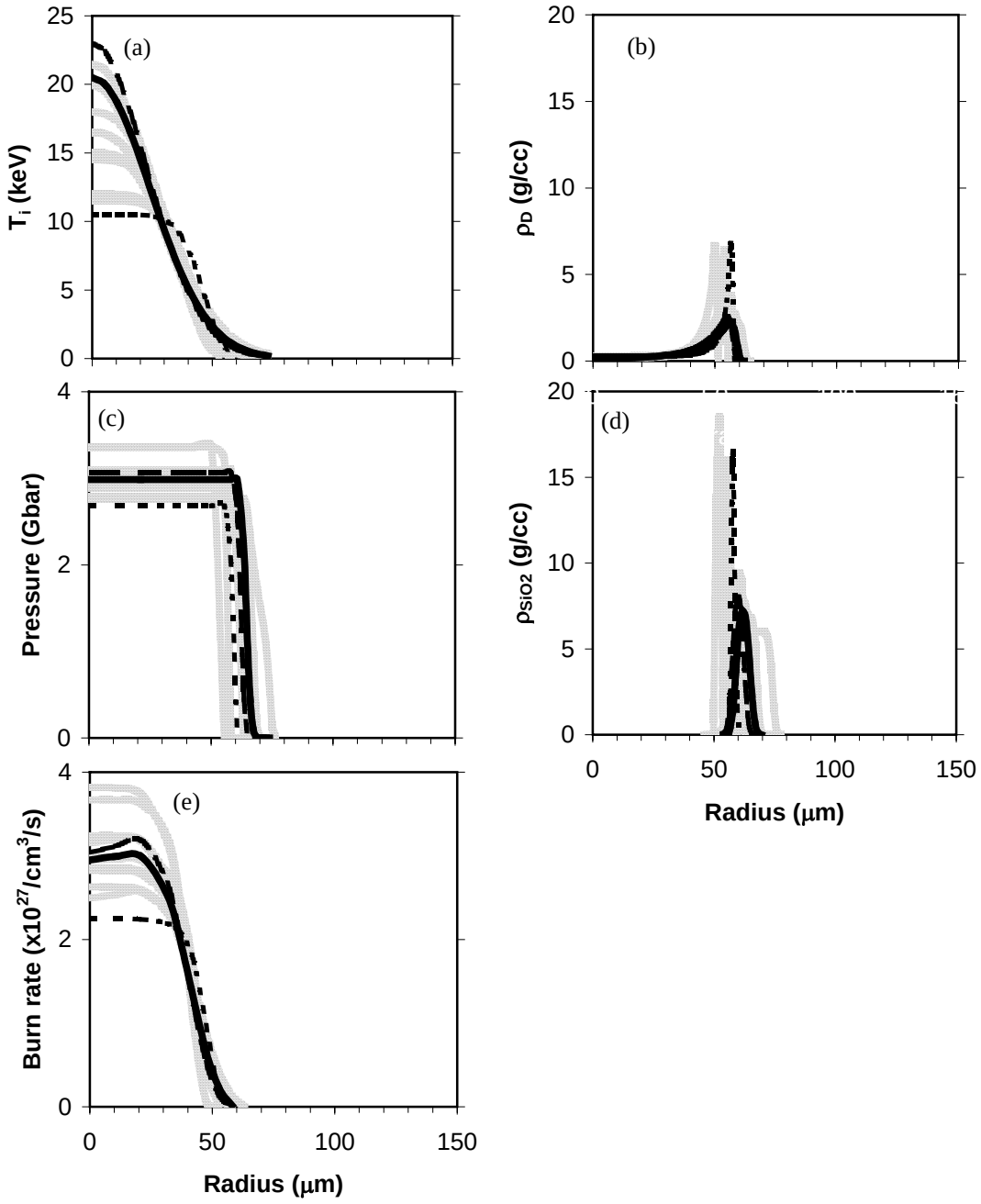

FIG. A.3 Samples of temperature, density, pressure, and burn profiles which produced fits to the data which were not as good as the best fit for implosion 30981. Bold lines represent the best-fit profiles; dashed and dotted lines represent the fits having the highest and lowest peak temperature, respectively, in the group of fits for which the total χ^2 is within one of its minimum value.

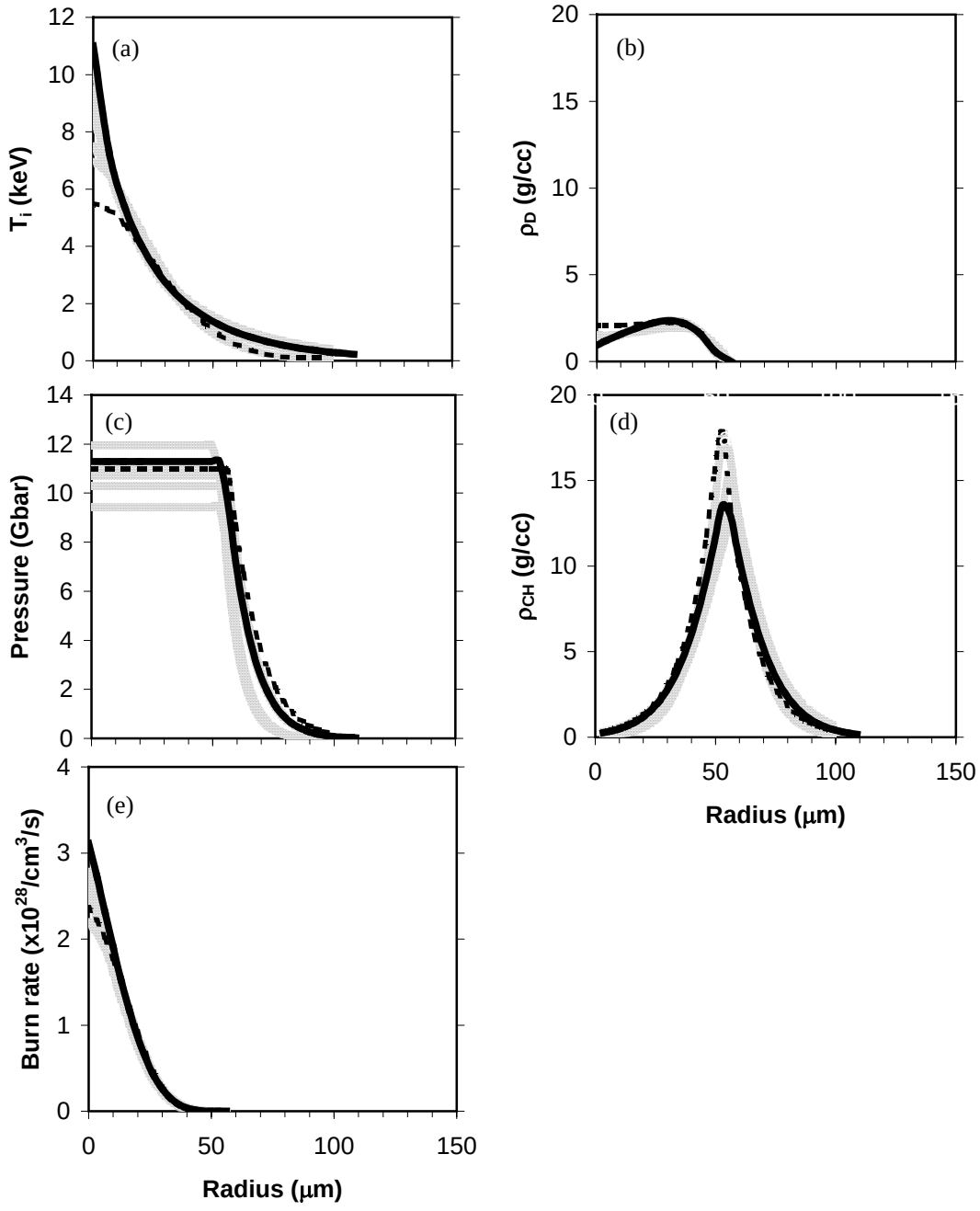

FIG. A.4 Samples of temperature, density, pressure, and burn profiles which produced fits to the data which were not as good as the best fit for implosion 27443 (as described in the caption of Figure A.3). The width of the burn profile is narrower than the width for implosion 30981, indicating more compression.

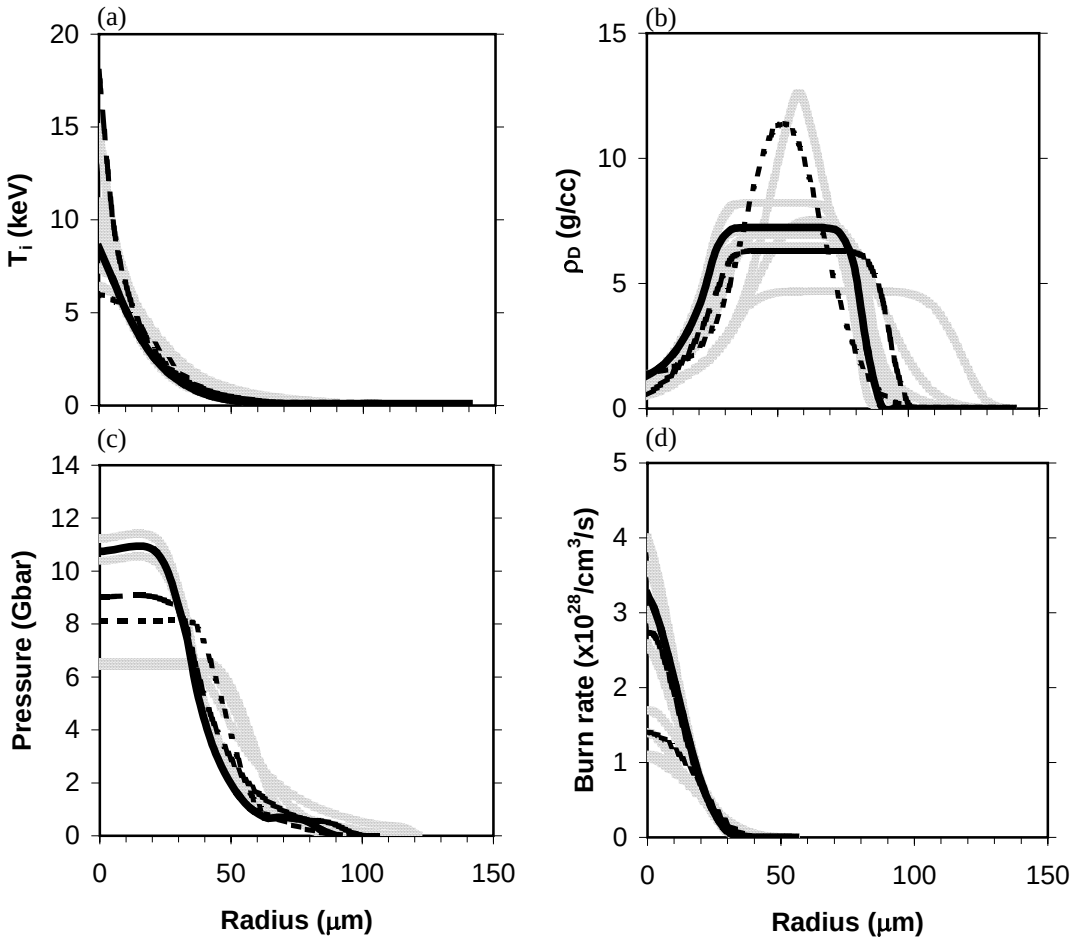

FIG. A.5 Samples of temperature, density, pressure, and burn profiles which produced fits to the data which were not as good as the best fit for implosion 28900 (as described in the caption of Figure A.3). The width of the burn profile is narrower than the width for implosion 30981, indicating more compression.